Supporting Information for

De novo automated design of small RNA circuits for engineering synthetic riboregulation in living cells

Guillermo Rodrigo[*], Thomas E. Landrain[*], and Alfonso Jaramillo[#]

[*] These authors contributed equally to this work
[#] To whom correspondence should be addressed. E-mail: alfonso.jaramillo@issb.genopole.fr

Contents

Extended Materials and Methods

Construction of RNA device plasmids

For the expression and characterization of the RNA species we used two different plasmid templates, pSTC0 and pSTC1 (Figs. S1 and S2). Both vectors were conceived to provide modularity in the construction of variants through restriction enzyme digestions and further ligations. The characterization plasmids, both pSTC0 and pSTC1, were made so that independent tunable promoters could drive the expression of the target mRNA (pLlacO-1[1] regulated by the LacI protein and the chemical inducer of the *lac* operon, isopropyl-β-D-thiogalactopyranoside, IPTG) and the expression of the sRNA (pLtetO-1 regulated by the TetR protein and the chemical inducer of the tetR operon, anhydrotetracycline, aTc), respectively (1). Both promoters were placed in opposite directions at a sufficient distance (122 bp between their respective start of transcription sites) in order to avoid transcriptional interferences (2). Of note, pSTC0 contained the pMB1 origin of replication (about 300 copies per cell, from pUC19), while pSTC1 contained the pSC101 origin of replication (about 5 copies per cell). Both plasmids contained the gene coding for kanamycin resistance. In the pSTC1 template we fused a strong RBS and the coding sequence of the red fluorescent protein (RFP) downstream of the sRNA terminator in order to monitor natural transcription termination efficiency from selected sRNA sequences. We used two variants of green fluorescent proteins, GFPmut3b (3) and superfolder GFP (sfGFP) (4), in pSTC0 and pSTC1 respectively, in order to monitor the translation rate of the transcribed mRNA. Absolute values of fluorescence for systems expressing GFPmut3b and sfGFP cannot be directly compared because of their difference in brightness. However, this precaution does not apply for comparing ratios of fluorescence values.

Before constructing the final plasmids, pSTC0 and pSTC1 were derived from the BioBrick (5) vectors pSB1AK3 and pSB4k5 respectively, and were modified so that a NheI restriction site appears between the start codon and the second codon of the green reporter gene. We also added a SpeI restriction site immediately after the ATG of the 5'-UTR. The RNA devices (from the terminator of the sRNA to the 5'-UTR of the mRNA) were made by DNA synthesis (DNA 2.0). Then, the RNA device cassettes were inserted by ligation into the vectors using the EcorI (BamHI) site downstream of the terminator of the sRNA for pSTC0 (pSTC1) and ligation of SpeI from the 5'-UTR to NheI from the reporter gene. The resulting scar is translated into Threonine and Serine, which are sufficiently inert amino acids to not alter the function of the reporter.

From the complete RNA devices, we generated Boolean derivatives by removing the sRNA operon using NheI (NheI and XbaI) digestion in pSTC0 (pSTC1), resulting in a vector bearing only the mRNA operon. We have used those Boolean derivatives for measuring the effect of the *trans*-activating RNA on its target. Additionally in pSTC1, the terminator of the sRNA could be removed by using two AvrII restriction site surrounding the terminator sequence.

---

[1] The sequence of pLlacO-1 we used was taken from the original Lutz and Bujard manuscript (1) in which the presented upstream lacO-1 operator was mistakenly exchanged with the lacO-2 operator (5'-aaatgtgagcggataacattgacattgtgagcggataacaagatactgagcac-3'). This has for consequence to make the promoter being slightly less repressed by LacI, resulting in a significant leakage of the mRNA expression when no IPTG is present. This explains why we see a significant up-regulation of GFP expression when aTc alone is added.

Basic molecular biology techniques were implemented as previously described (6). Characterization of GFP expression was done using fluorometry and flow cytometry, as two independent methods.

RNA quantification by RT-qPCR

Overnight LB cultures (shaking at 200 rpm at 37°C) were diluted 1:100 into fresh media and then incubated for 2 h. 2 mL were used for RNA extraction. Cells were pelleted by centrifugation at 5,000 rpm for 10 min, 600 μL of lysis buffer was added, and then cells were incubated with shaking at room temperature for 5 min. After subsequent centrifugation at maximal speed, supernatants were transferred to 330 μL of 96% ethanol, and then centrifuged again at 10,000 rpm. Two washes with commercial buffers were carried out by centrifuging at 10,000 rpm for 30 s. Total RNA was eluted in 30 μL of a commercial buffer and quantified in a NanoDrop.

One-step SYBR PrimerScript RT-PCR Kit II (Takara) was used for detection, following the Kit protocol for preparing the reaction volumes. 16S rRNA was used as housekeeping gene to normalize RNA quantity in each reaction. GFP mRNA was used to calculate the ratio between the two RNA species. The primers for RT-qPCR were synthesized by Sigma. The primer sequences for amplifying transRAJ11 were designed with Primer3 (http://frodo.wi.mit.edu) (7) and were 5'-GGGAGGGGTTGATTGTGTGAG (forward) and 5'-ATCAACGTTTCCGCTGAACT (reverse), for GFPmut3b, taken from (8), were 5'-ATGGAAGCGTTCAACTAGCAGAC (forward) and 5'-CGAAAGGGCAGATTGTGTGGAC (reverse), and for 16S rRNA, taken from (9), were 5'-GTGGCATTCTGATCCACGATTAC (forward) and 5'-CCGGATTGGAGTCTGCAACT (reverse). Reactions in triplicate were carried out using a 7500 Fast Real-Time PCR System (Applied Biosystems). The thermal cycling program for amplification was 5 min at 42°C, 10 s at 95°C, and 40 cycles of 5 s at 95°C and 34 s at 60°C (Shuttle PCR); following with default melting curves.

Our results for system RAJ11 show that the GFP mRNA (normalized by the amount of 16S rRNA) is similar in absence or presence of sRNA, indicating that the increase in fluorescence is not due to an increase in transcription rate. To elucidate the observed increase in fluorescence in the HT115 strain (containing a RNase III knockout), we measured the ratio sRNA/mRNA, observing that it did not increase in the strain HT115 (compared against the strain JS006). Although this result does not explain the observed increase in apparent activation fold in the HT115 strain, a more thorough clarification goes beyond the goals of the present work.

Computation of apparent activation fold

To compute the apparent activation fold we took the ratio of the normalized fluorescence signals without subtracting the auto-fluorescence of the system. Normalized fluorescence was calculated as the slope of the linear regression between absolute fluorescence and OD_{600} (10-12). Due to the high efficiency of the *cis*-repressing modules, the level of fluorescence from the mRNA alone overlaps with the one from the negative control. If we were to subtract values of auto-fluorescence in *cis*-repressed systems, we would obtain values too close to zero (even negative due to stochasticity) to be considered as relevant denominators for computing absolute activation folds, otherwise too sensitive to noise. This apparent activation fold represents a systematic under-estimation of the real efficiency of our systems.

Algorithm for sequence optimization

Riboregulation is based on conformational changes in the secondary structures of RNA molecules that allow controlling protein expression. In that way, the proper function of an sRNA-based circuit relies on the structures of all species, since a disruption of the precise fold may result in a non-functional RNA, then affecting the circuit behavior. We assume that the annealing between two RNAs is rate limited by the formation of an intermediate complex (e.g., kissing loops) involving the nucleotides that are not paired in each interacting species. Then, the stems next to that binding site from both RNAs are destabilized to form a complex, most often with unrelated secondary structures to their initial ones. We did not account for the kinetics of the folding process. We assumed it is a fast process, since its

time scale is of microseconds whereas hybridization takes seconds or even minutes (14). Hence, we assumed that prior to the hybridization RNA molecules fold into their structures.

In our computational approach, the structures of all single species are imposed as design specifications. To address the computational design, we have to find the sequences folding into the predefined structures that would interact specifically among them to form predefined complexes displaying a targeted behavior. The structural constraints are exploited to considerably reduce the combinatorial space and accelerate the design of nucleic acid sequences. Our computational procedure optimizes at the same time all RNA sequences of the circuit. During the optimization we do not need to impose constraints derived from natural sequences, such as stems with high GC-content or loops with YUNR motifs (consensus UUGG), which have been found in natural systems (15,16). On the other hand, we could add specific RNA motifs for specific RNA-protein interactions with RNA chaperones (like Hfq) or RNAses (like RNase III). Importantly, our designs are just based on low-level physicochemical principles and not on additional fitting, thus allowing their reliable implementation in a given cellular chassis.

The optimization algorithm we have developed consists in a Monte Carlo Simulated Annealing (17); see scheme in Fig. S3. Our approach consists in optimizing an objective function accounting for the stability of the RNAs and the kinetics of the reactions that lead to the target behavior. To compute the energy and folding (we assume that the secondary structure would be sufficient) of all species and complexes of a system, we have used the ViennaRNA (18,19) and MultiRNAFold (20) packages. We used ViennaRNA to compute the energies and structures of the single species, whereas MultiRNAFold the energies and structures of the complexes. In this work, we always have considered T=37 °C (kT=0.61 Kcal/mol).

The design specifications comprise the secondary structures of all single RNAs, any nucleotide subsequence that is held fixed (e.g., RBS), the reaction kinetics, and the structure of the output complex. The algorithm starts from random sequences satisfying the structural and subsequence constraints. If the subsequence constraints do not allow satisfying the structures, the algorithm stops. The algorithm allows relaxing the constraints, for instance by imposing a tolerance allowing species to adopt similar structures than their initial specifications. Afterwards, an iterative process of mutation and selection is implemented. The mutation moves involve randomly replacing one or two nucleotides if the position corresponds to an unpaired or paired conformation respectively. If a nucleotide that has to be mutated belongs to a stem, it is also mutated its pair in the stem with the corresponding nucleotide with the aim of preventing the disruption of the secondary structure and improving the convergence. We avoid sequences having consecutive repeats of four or more identical nucleotides (13). To speed up the sequence search we have introduced a mutation move involving a complementary word exchange between two interacting strains. For this we take a set of consecutive nucleotides (which we call word) from one sequence, making its reverse complement, and randomly inserting it into another sequence. This process intends to accelerate the creation of interacting species by enhancing the complementarities between strands. Initially, the length of this word is three, and it is reduced to one (i.e., single point mutation) during the optimization process. We do not consider additions or deletions.

Our optimization corresponds to a minimization problem with an objective function defined as the sum of the free energy of complex formation and the energy for the activation barrier. For that, we compute the free energy of complex formation (ΔG_{ij}) and the length of the toehold (α) of all targeted pairwise interactions ij (21-23), having

$$\Delta G_{\text{interaction } ij} = \begin{cases} \Delta G_{ij} + \alpha_{ij} G_p, & \text{if no interaction is targeted (OFF)} \\ \min(0, \Delta G_{\text{sat}} - \Delta G_{ij}) + G_p \max(0, \alpha_{\text{sat}} - \alpha_{ij}), & \text{if interaction is targeted (ON)} \end{cases}$$

(Eq. S1)

where ΔG_{sat}=-15 Kcal/mol and α_{sat}=6 (saturation levels). G_p=-1.28 Kcal/mol is the average contribution of a nucleotide in the toehold to the free energy of the initiation process (22). The specification of the possible interactions among strands serves to define the behavior of the system. In case of the design of riboregulators (Fig. S4), involving two RNA species (RNA1 and RNA2), three possible interactions can occur: (a) RNA1+RNA1, (b) RNA2+RNA2, and (c) RNA1+RNA2,

discarding higher-order combinations. Thus, the homodimers (a) and (b) must be OFF and the interaction (c) ON. In other words, in our riboregulator example, we will optimize the formation of the heterodimer while restraining the homodimer. The algorithm can be used for the design of circuits involving more than two RNA species. In the case of considering three species (Fig. S21), we account for dimers and trimers, while discarding higher-order combinations.

We have also introduced a new term to the objective function to allow relaxation of the specifications and constraints. Such term allows improving the convergence and it should end up being zero once all the constraints are obeyed. For this, we use a Hamming distance (d) between the current and target structures of the RNA species and of the RNA complex. For the latter, we specify the target structure by allowing any complex structure provided the RBS sequence nucleotides are unpaired. To maximize the translation rate, we also enforce that the four nucleotides upstream the RBS and all downstream nucleotides be unpaired in the final hybridized structure.

$$\Delta G_{\text{constraints}} = d_{\text{target, complex}} G_p . \qquad \text{(Eq. S2)}$$

Thus, by selecting the λ factor between 0 and 1 (we usually select $\lambda=0.5$), we can scalarize the problem resulting in

$$\Delta G_{score} = \lambda \sum_{i,j} \Delta G_{\text{interaction}\,ij} + (1 - \lambda)\Delta G_{\text{constraints}}. \qquad \text{(Eq. S3)}$$

The algorithm converges rapidly ($\Delta G_{\text{score}} \rightarrow 0$) following an exponential scale (Fig. S5) and it can be launched in personal computers. It can be also launched in parallel in supercomputers to obtain multiple designs.

Thermodynamic ensemble and energy gap

RNA molecules can fold into an ensemble of alternative structures. The free energy of each conformation (assuming 0 for the unfolded state) determines its probability of occurrence within the constant temperature statistical ensemble. Our algorithm, instead of accounting for the whole ensemble, only considers the contribution from the minimum energy conformation (MEC). This approximation is necessary to make feasible the optimization problem and it could be justified in those cases where it exists an energy gap between the MEC and any suboptimal structure. We expect that the optimization itself would already provide such a gap because the score used in the optimization is proportional to the MEC energy. This implies that we are finding sequences with decreased MEC energy while the suboptimal states. This is of special interest for the formation of the complex. We have observed that reactions with moderated values of ΔG (about -5 Kcal/mol) do not ensure the major formation of the complex at the equilibrium. For that, lower values of ΔG are required (about -15 Kcal/mol).

Once the complex is formed, we have to calculate the release of the RBS. In our algorithm we just do so for the complex with minimum free energy. However, as we know, there is an ensemble of structures for the complex. The sequences of the solutions were further analyzed with the software package NUPACK to check their statistical ensemble (21), which we modified to calculate the probability of finding the RBS unpaired throughout the conformations of the thermodynamic ensemble (P_{rbs}). This probability accounts for the total number of structures that effectively released all nucleotides of the RBS sequence. More intuitively, we could already use the pair probability maps (24) to estimate such probability. In fact, we could do this by picking the nucleotide i for which the probability that a given nucleotide i of the RBS is unpaired (P_{rbs_i}). Fig. S10 shows a correlation of such quantity with P_{rbs}.

In addition, a mutational analysis showed that most of the nucleotides of the species sequences have a moderated impact on the device performance, whereas there are key nucleotides whose mutations provoke the total malfunction of the device (Fig. S8). We also showed that the toehold sequence is a critical region for the performance of the device. Mutations in it reduce significantly the

specificity of the RNAs (Fig. S9). This fact may be exploited to apply manual design techniques to obtain a library of new systems.

Limitations of the approach

One limitation of our approach is the use of the secondary structure to model the RNA molecule. Three-dimensional models could better capture the interaction features of molecules (25-27). Our methodology could be coupled with a 3D prediction procedure once the optimization process using secondary structures had yielded a sufficiently good set of solutions according to the specifications. Another limitation relates to the uncertainty coming from premature/inefficient transcription termination in our RNA sequences. Either the sRNA already encodes a transcription terminator, or we place it manually. In fact, each hairpin may already induce some termination. The process of transcription termination produces a population of sRNAs with different lengths, either due to a premature or inefficient (the last hairpin may not terminate always) termination, which may influence the folding of the global structure and its ability to interact properly. Consequently, we could include into the objective function predictors of transcription termination (28) to better target a more homogeneous population. A limitation in using our generic objective function to design translational activators is that is that our objective function is not a direct measure of activation fold. Another limitation of the current method is the enforcement of a given structure for all single species in the circuit. Although these structures serve to gain stability, this constrains the sequence space of possible solutions (29). We have to note here that we do not impose a particular structure for the complex species; we just introduce into the objective function a term to account for an appropriate conformational change (e.g., RBS free in the complex species). The enforcement of structures has not been a problem for the computational design of YES (Fig. S7) and even AND gates (Fig. S21), but it could be an obstacle to find the sequences implementing more complex behaviors. It could be possible to leave unconstrained the secondary structure of each single species and include into the structural term ($\Delta G_{\text{constraints}}$) the intended molecular function (e.g., *cis*-repression in case of 5'-UTR) and the stability (through a folding free energy term). In such a way, we could also perform additions and/or deletions (not only replacements) of nucleotides during the optimization. Moreover, as the complexity of the function in the RNA circuit increases (e.g., from YES to higher order logic gates), we require the use of more sophisticated search algorithms to improve the convergence. It could be possible to reuse functional RNAs (or at least use them as starting points for our *in silico* evolution) to design higher order logic circuits and then reduce the sequence space. Despite of this, a further limitation of the current method is that it only allows designing static systems (i.e., in steady state) and it does not allow designing, for example, an RNA-based oscillator. To this end, we would need to account for k_{on}, k_{off} and k_{cat} for all reactions to construct a model based on differential equations (23,30). Finally, our procedure could be extended to provide a combinatorial library of sequences to be used for screening or directed evolution. We plan to address these issues in our future work.

Mathematical model of the AND circuit

The two promoters of the system (PLlacO-1 and PLtetO-1) can be modeled by using Hill-type equations (31,32), relating the expression of the two repressors (LacI and TetR) and their corresponding inhibitors (IPTG and aTc). Thus, the transcription rates read

$$P_m(LacI, IPTG) = P_m^{\,0} \frac{1 + 1/f_{lac}\left(\dfrac{LacI}{K_{lac}\left(1 + IPTG/K_{IPTG}\right)}\right)^{n_{lac}}}{1 + \left(\dfrac{LacI}{K_{lac}\left(1 + IPTG/K_{IPTG}\right)}\right)^{n_{lac}}} \qquad \text{(Eq. S4)}$$

and

$$P_s(TetR, aTc) = P_s^0 \frac{1 + 1/f_{tet}\left(\dfrac{TetR}{K_{tet}\left(1 + aTc/K_{aTc}\right)}\right)^{n_{tet}}}{1 + \left(\dfrac{TetR}{K_{tet}\left(1 + aTc/K_{aTc}\right)}\right)^{n_{tet}}} \qquad \text{(Eq. S5)}$$

where P_m^0 and P_s^0 are the maximal transcription rates, f_{lac} and f_{tet} the repression folds, K_{lac}, K_{tet}, K_{IPTG}, K_{aTc} the effective binding coefficients, and finally n_{lac} and n_{tet} the Hill coefficients. Therefore, we can construct a system of ordinary differential equations (12,33) given by

$$\frac{d}{dt}mRNA = CP_m(LacI, IPTG) - (\mu + \delta_m)mRNA$$

$$\frac{d}{dt}sRNA = CP_s(TetR, aTc) - (\mu + \delta_s)sRNA \qquad \text{(Eqs. S6)}$$

$$\frac{d}{dt}GFP = \left[r_0 mRNA_{free} + r_1 sRNA::mRNA\right]\frac{m}{m + \mu + \delta_g} - (\mu + \delta_g)GFP$$

where C represents the plasmid copy number, μ the cell growth rate, δ_m and δ_s the RNA degradation coeffcients, δ_m the fluorescent protein degradation coefficient, and m its maturation rate. As above, r_0 is the mRNA translation rate (basal) and r_1 the sRNA::mRNA translation rate. By noting that the composition of two Hill functions also results in a Hill function, we can simplify the model to derive the GFP expression in steady state. According to our experimental results (Figs. S13 and S15), in absence of both inducers the system expresses a very low amount of protein (low leakage).

Applying renormalization of parameters, we propose a model for the regulatory system, which can be used to predict the corresponding response surface. This model only accounts for the concentrations of IPTG and aTc, given that LacI and TetR are constitutively expressed by the cell. In addition, the regulation by sRNA is enclosed within the parameters for aTc. This model reads

$$GFP_{ss}(IPTG, aTc) = F_0 \frac{1 + f_1\left(\dfrac{IPTG}{K_1}\right)^{n_1} + f_2\left(\dfrac{aTc}{K_2}\right)^{n_2} + f_1 f_{sRNA}\left(\dfrac{IPTG}{K_1}\right)^{n_1}\left(\dfrac{aTc}{K_2}\right)^{n_2}}{1 + \left(\dfrac{IPTG}{K_1}\right)^{n_1} + \left(\dfrac{aTc}{K_2}\right)^{n_2} + \left(\dfrac{IPTG}{K_1}\right)^{n_1}\left(\dfrac{aTc}{K_2}\right)^{n_2}} \qquad \text{(Eq. S7)}$$

where F_0 is the normalization parameter. In this model, IPTG and aTc act independently each other. From Lutz and Bujard work (1), we obtained $K_1 \approx 35$ µM, and $K_2 \approx 5$ ng/mL. From our own data (Fig. 5C), we estimate $K_1 \approx 15$ µM, $K_2 \approx 3$ ng/mL, $n_1 \approx 2$, $n_2 \approx 1.5$, $f_1 \approx 1.2$, $f_2 \approx 1.5$ and $f_{sRNA} \approx 8.3$ (for system RAJ11, taking $F_0 = 1$). These values should be nevertheless taken with caution because there were fitted against estimators of activation fold. The absolute activation fold of system RAJ11 is $f_{sRNA} \approx 11.2$ according to Fig. 2. This discrepancy in activation fold, although not significant, can be rationalized. While in strain JS006 (a derivate of MG1655) we take the intracellular steady state of the system, in strain MG1655-Z1 we deal with dynamical effects because IPTG and aTc inhibit with time the activity of the highly expressed repressors. This forces to use different methods to obtain the value of activation fold. With JS006, we obtain a better characterization of the performance of the system by applying regression over multiple states, which allows averaging noise in gene expression. With MG1655-Z1, we need to avoid the transient dynamics and take the steady state value after several hours. There, the population may enter into stationary phase before our system reaches its steady state, hence we expect to under-estimate the normalized fluorescence. Thus, to construct the prediction shown in Fig. S20 we replace 8.3 by 11.2 in f_{sRNA}, while keeping the other parameter values.

Supporting Figures
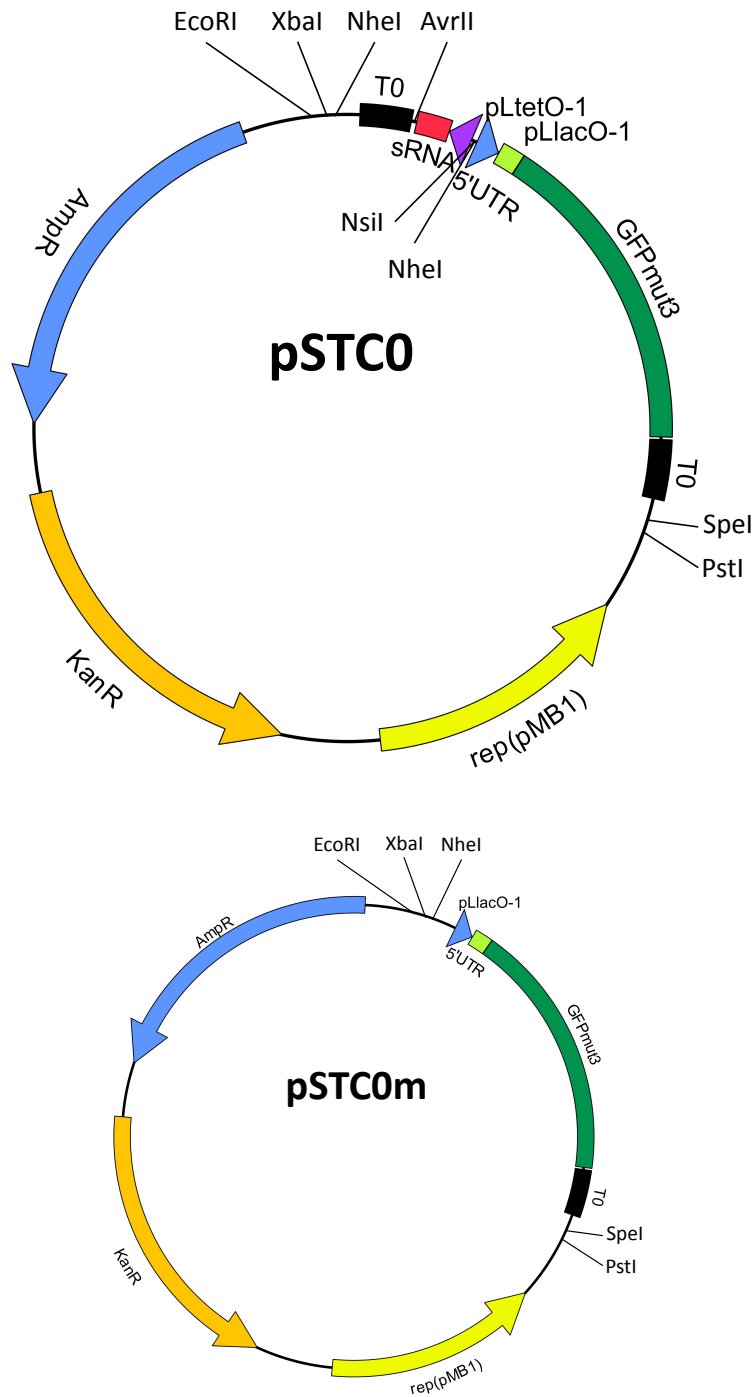
Fig. S1: On the top, scheme of the vector pSTC0 used to express our RNA devices in bacteria (obtained with ApE). The sRNA for *trans*-activation comes in reverse direction, while the *cis*-repressed mRNA of GFP in forward. T0, BBa_B0015 terminator. On the bottom, scheme of a derivative vector pSTC0m used to only express the *cis*-repressed mRNA of GFP. The pSTC0m was made digesting the pSTC0 with NheI and religating.
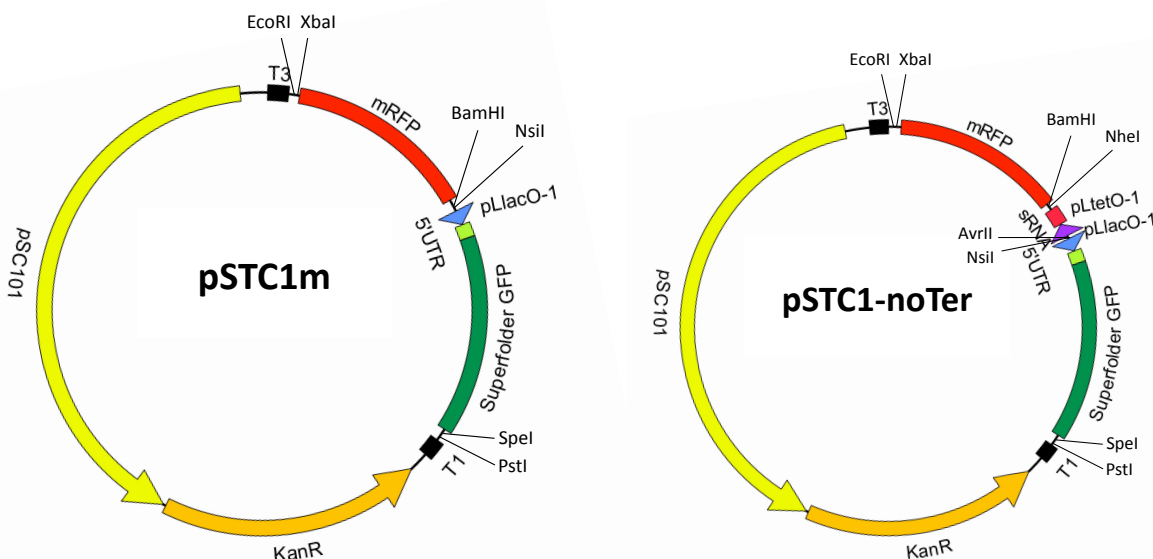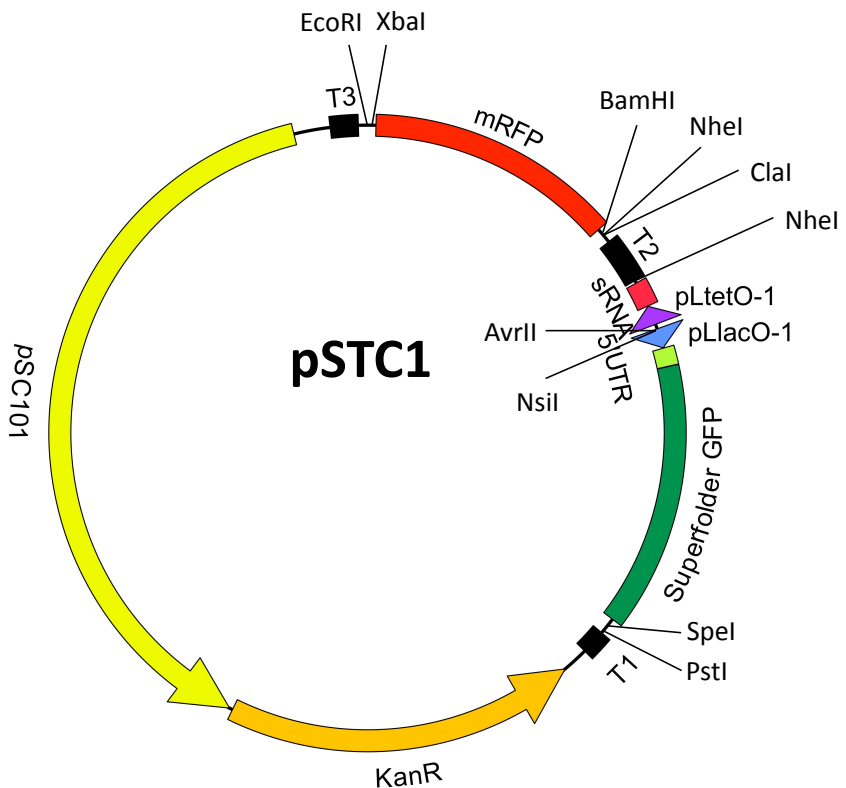
Fig. S2: On the top, scheme of the vector pSTC1 used to express our RNA devices in bacteria (obtained with ApE). The sRNA for *trans*-activation, followed by the mRNA of RFP, comes in reverse direction, while the *cis*-repressed mRNA of GFP in forward. T1, BBa_B0054 terminator; T2, BBa_B1002 terminator; T3, BBa_B0055. On the bottom, schemes of the derivative vectors pSTC1m and pSTC1-noTer used to only express the *cis*-repressed mRNA of GFP and to express the sRNA without transcription terminator, respectively. The pSTC1m was made by digesting the pSTC1 with NheI and AvrII and religating. The pSTC1-noTer was made by digesting the pSTC1 with NheI and religating.
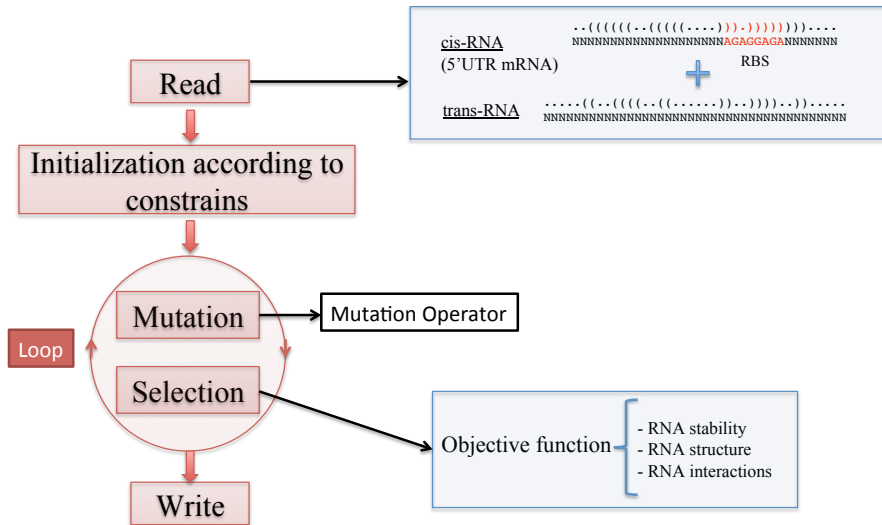
Fig. S3: Scheme of the Evolutionary Algorithm used to design/optimize the RNA sequences that implement a riboregulatory circuit. Starting from random or specified sequences, satisfying the kinetic and structural constraints, the algorithm generates a population of sequences that evolve in parallel against an objective function that accounts for stabilities, structures and interactions of the RNAs. The algorithm is based on a Monte Carlo Simulated Annealing optimization scheme.
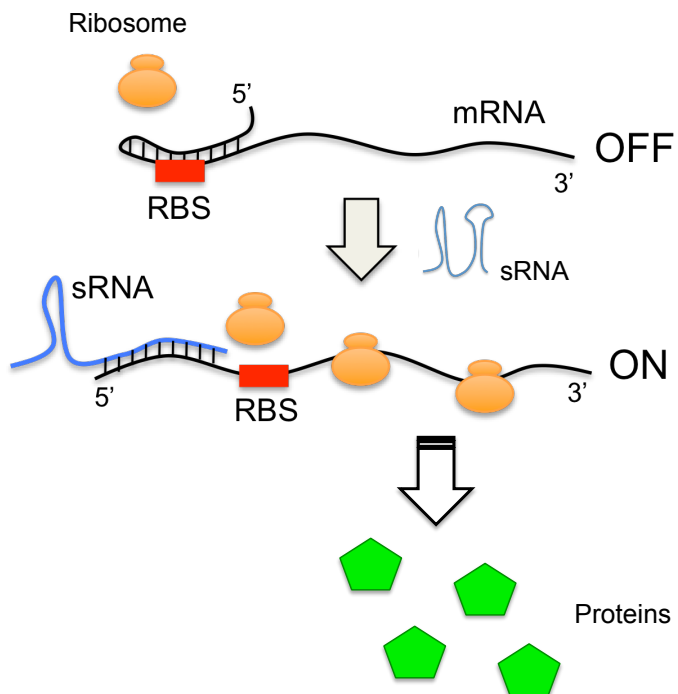
Fig. S4: Scheme of the mechanism of control exerted by riboregulators. The *cis*-repressing RNA forms a hairpin that prevents ribosome binding and then blocks translation (riboswitch). The *trans*-activating RNA is a small RNA (sRNA) that can change the structural conformation of that riboswitch thus releasing the RBS and allowing protein production.
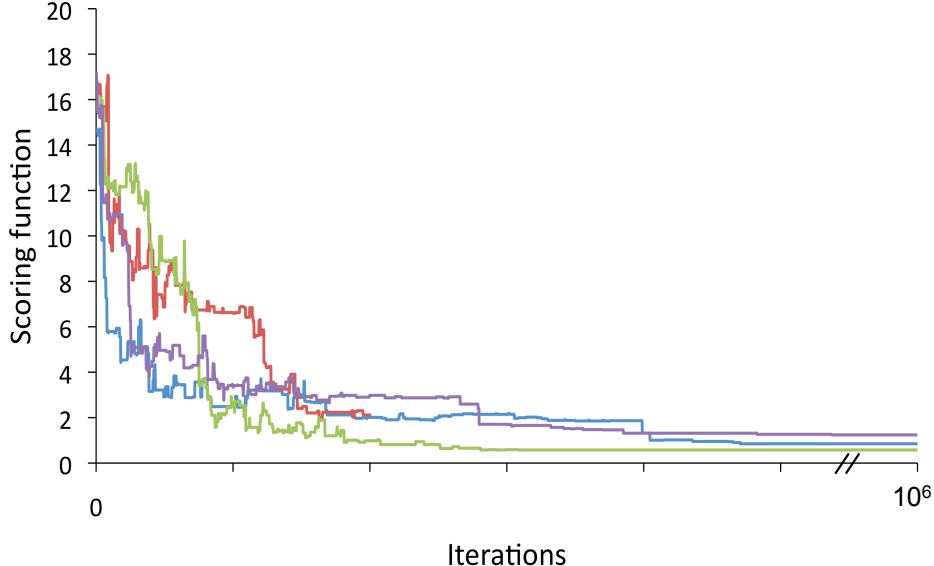
Fig. S5: Illustration of the convergence of the algorithm. We show the evolutionary path of three different random sequences (exploring the fitness landscape) under the selection pressure imposed by the scoring function accounting for the interaction and allosteric regulation of the RNAs. We follow an exponential cooling schedule.
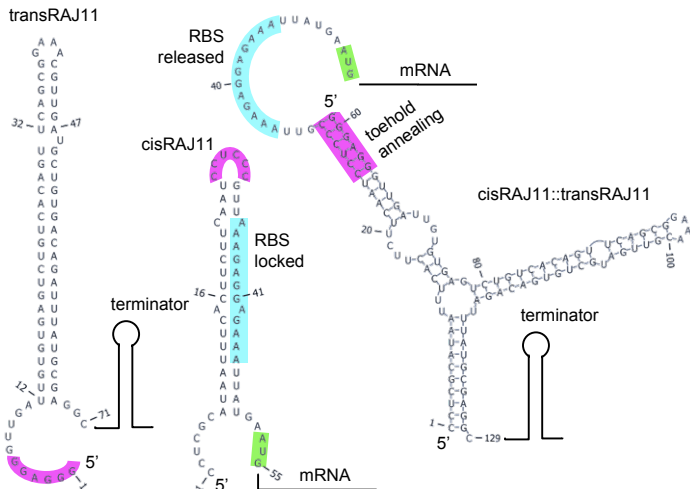
Fig. S6: Illustration of the RNA device RAJ11. Sequences and secondary structures of the species of the system (cisRAJ11, transRAJ11, and the complex cisRAJ::transRAJ11). The RBS is colored in cyan, the toehold in magenta, and the start codon in green. Nucleotides are numbered relative to the predicted natural transcription start site; in the complex, transRAJ11 is numbered consecutive to cisRAJ11. The conformational change induced by the riboregulator release the RBS to activate translation.

11
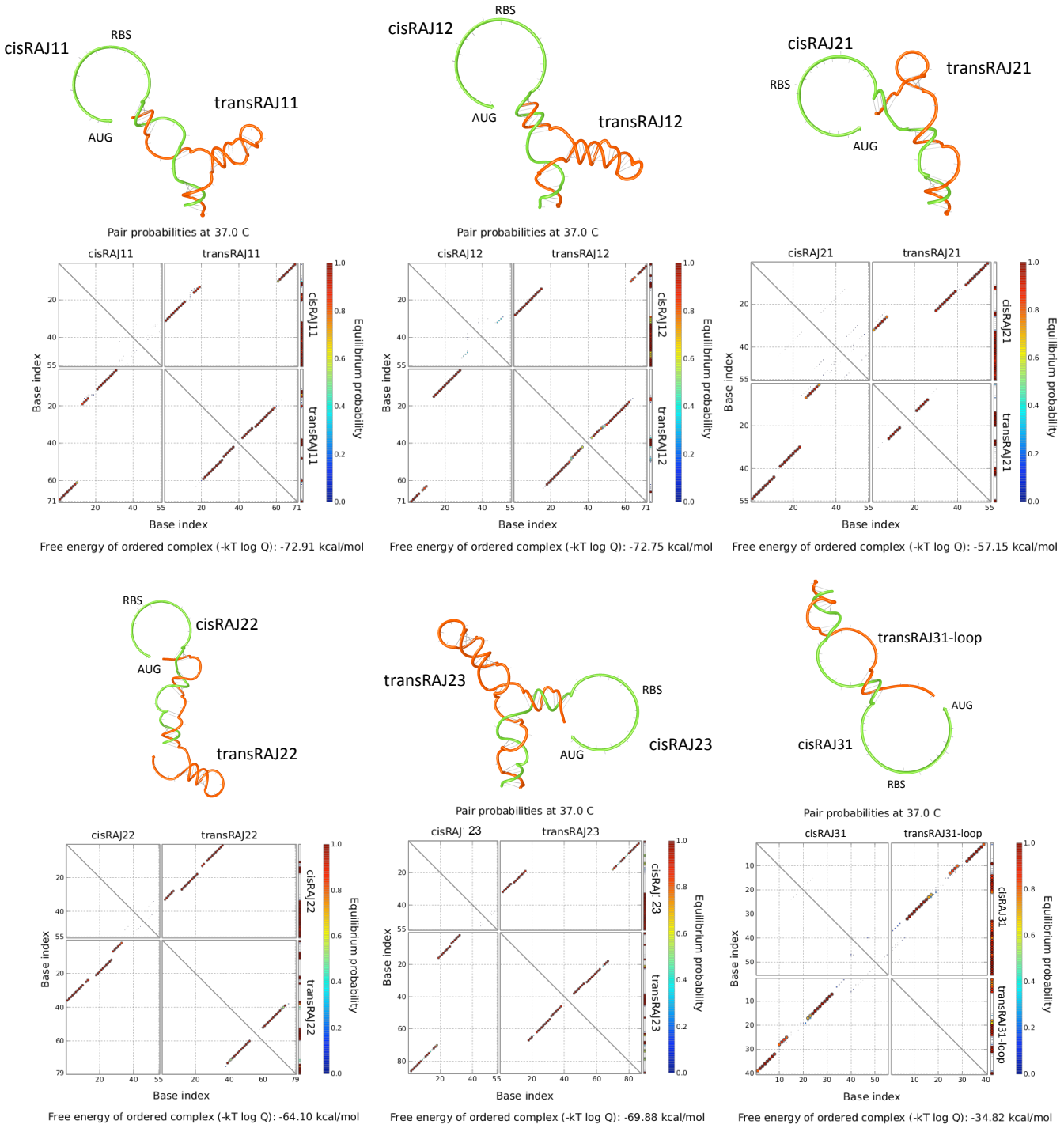
Fig. S7: Helical structure of the two-RNA-strand complexes, showing the release of the RBS, together with the corresponding base-pairing probability matrix. Plots carried out with NUPACK. In the case of RAJ31, we just consider the loop of the *trans*-RNA to avoid working with pseudoknots. We assume that the large stem of transRAJ31 is very stable and then it is not altered in the interaction, where the loop plays the regulatory role, as done in (34). We also verified that the interaction agrees with a calculation including pseudoknots with IntaRNA (35).
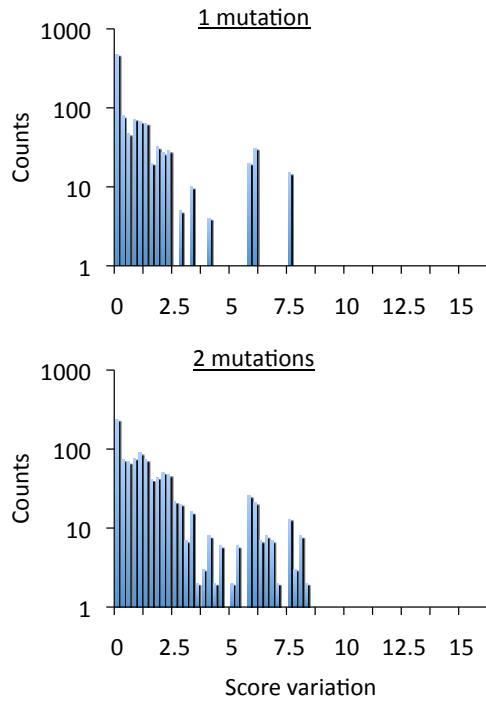
Fig. S8: Mutational fitness landscape for the system RAJ11, computed with 1000 simulations. Our score comes from a minimization problem (global optimum at 0 in case of existence). The average score variation for one mutation is 0.859 and for two mutations 1.547. In addition, the probability of a neutral mutation is 0.476 (score variation = 0), of a deleterious mutation 0.410 (0 < score variation <= 2), and of a lethal mutation 0.114 (score variation > 2). As expected from a Simulated Annealing optimization, there are no beneficial mutations or eventually their probability is extremely low. Similar distributions were found for the other RNA systems.
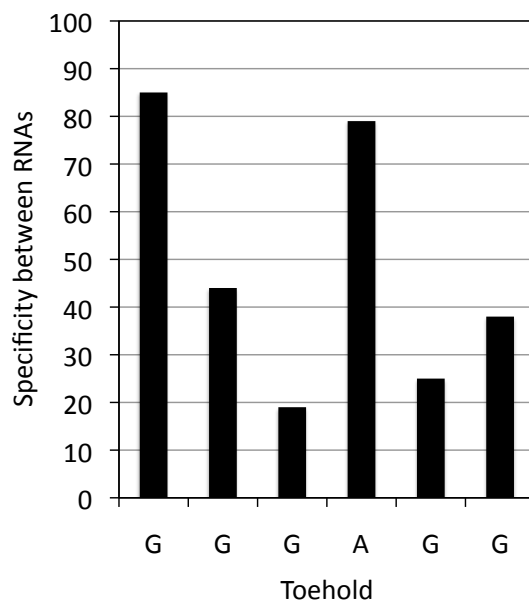
Fig. S9: Computational prediction of the specificity of the RNA strands (*cis* and *trans*) of the device RAJ11 when mutating the nucleotides of the toehold (we show the sequence of transRAJ11). The third and fourth Gs show the greatest sensitivity.

13
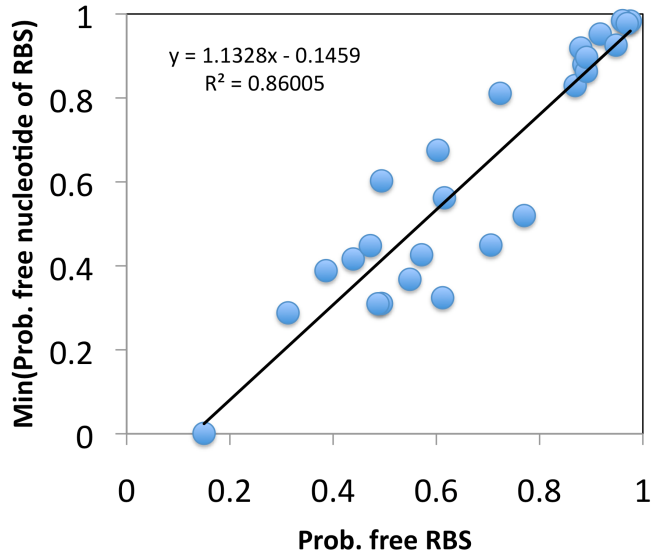
Fig. S10: Correlation between the probability of free RBS (P_{rbs}) and the minimum probability of a free nucleotide within the RBS sequence (P_{rbs_i}). To perform this plot, we used a large set of computational designs.
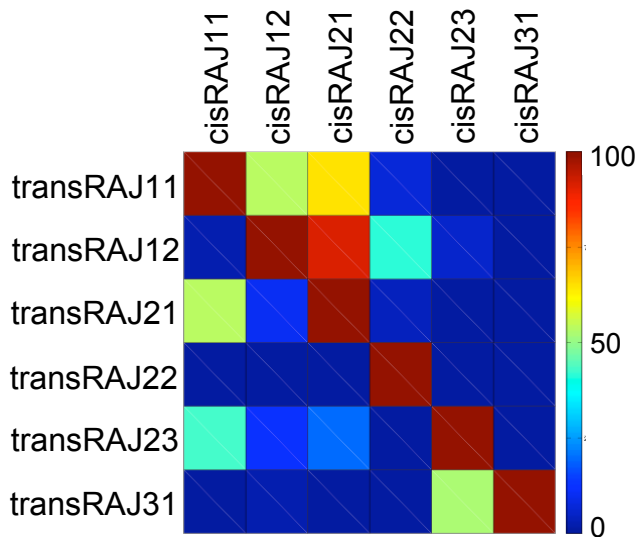
Fig. S11: Computational prediction of orthogonality of the devices, showing the probability of complex formation at the equilibrium when both species have an initial concentration of 100 μM. In Fig. 4B (main text) we used an initial concentration of 1 μM.
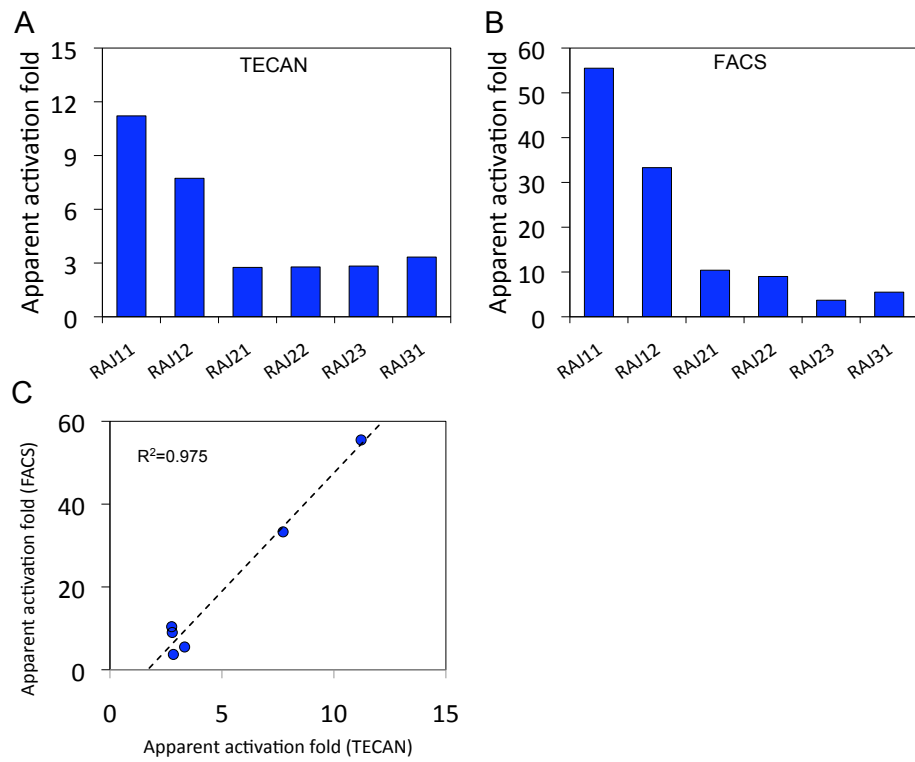
Fig. S12: (A, B) Apparent activation fold of the RNA devices according to fluorescence data (fluorometry and flow cytometry). Ratio of fluorescence values in presence of the riboregulator and in absence of it. (C) Correlation between the two experimental magnitudes, showing a high agreement.
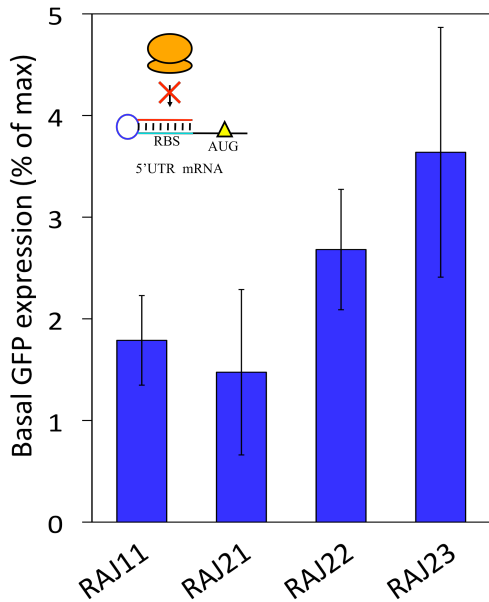
Fig. S13: Characterization of the *cis*-repression activity of the 5'-UTR of the mRNA (for systems expressed in pSTC0), relative to the maximal expression achieved without *cis*-repression corresponding to the 100%.
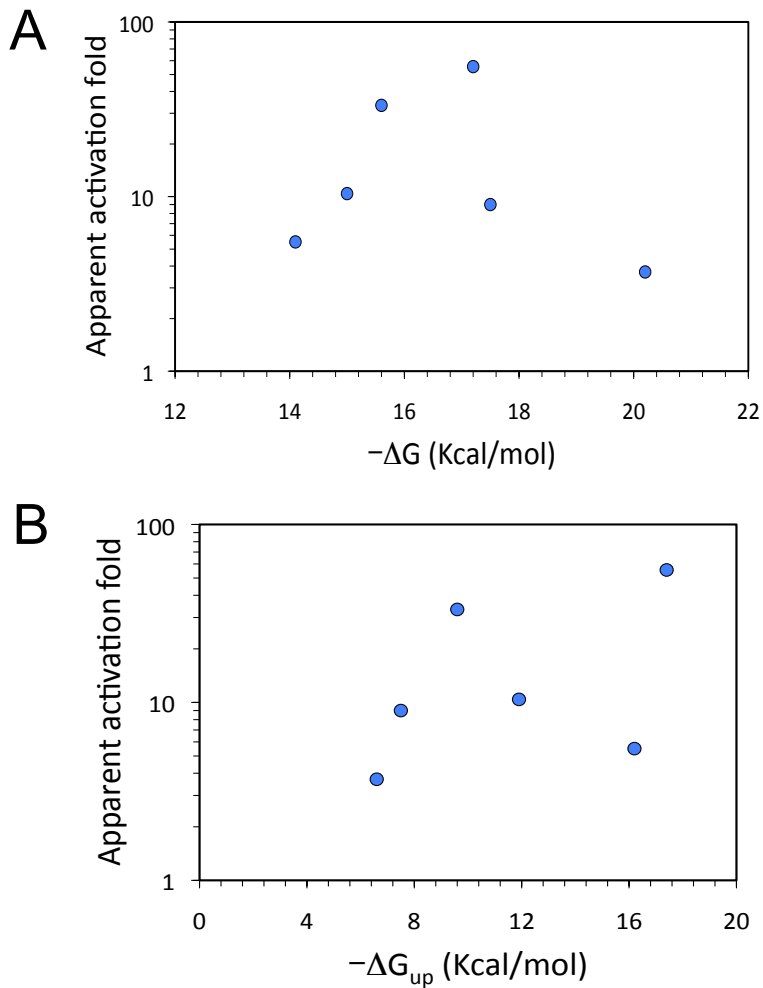
Fig. S14: Scatter plots between the apparent activation fold (according to flow cytometry) and (A) the free energy release of the reaction according to NUPACK (ΔG) and (B) the free energy release of the interaction according to RNAup (ΔG_{up}) (36). In these cases, we do not find a clear correlation. However, our analysis of previous riboregulators (R7, R10 and R12) engineered by Collins and coworkers (37) shows that differences in fold can be explained by a simple exponential model with ΔG (fold-change obtained from FACS data, f=[1, 8, 19] and ΔG=[3.6, 12.9, 15.1] Kcal/mol, with R^2=0.99 and P-val=0.14). Even though, in recent work coupling aptamers with small RNAs by Arkin and colleagues (38), ΔG results in a partial estimator of activity, pointing out that the stability of the small RNA plays also a relevant role.

16
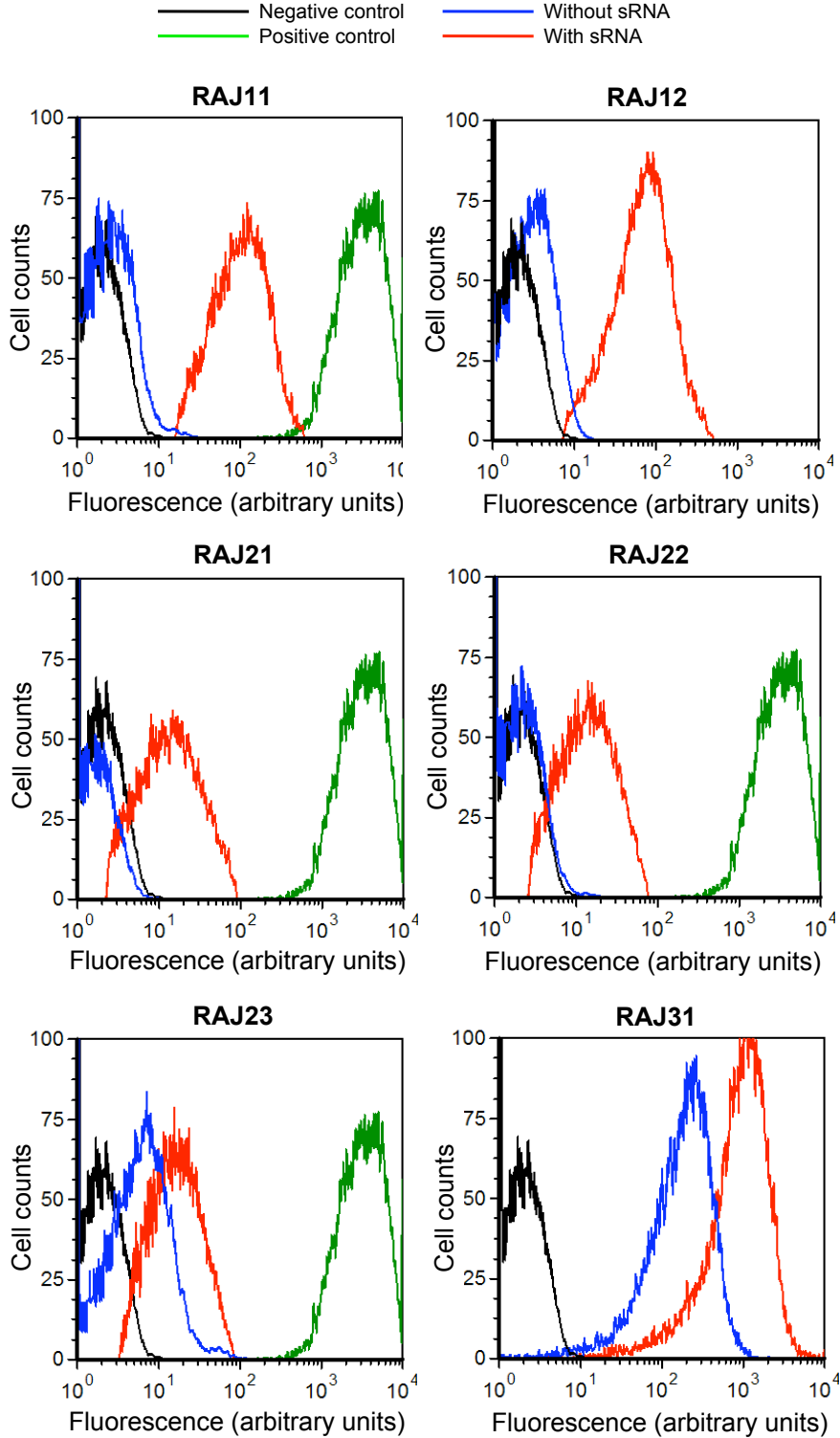
Fig. S15: Flow-cytometric results for all RNA devices in JS006. The negative control (black) corresponds to cells carrying a plasmid without RBS in the 5'-UTR of the mRNA (pSTC0r0). The positive control (green) corresponds to cells carrying a plasmid without *cis*-repression for GFP (pSTC0r1). This positive control corresponds to the expression of GFPmut3, and then it cannot be used as reference for devices RAJ12 and RAJ31 expressing superfolder GFP. The blue curve represents *cis*-repressed cultures (no sRNA). The red curve corresponds to cells expressing the sRNA able to activate GFP translation. Of note, the devices show in all cases high *cis*-repression and significant *trans*-activation. In all cases, we obtained statistical values of significance of $P<10^{-5}$ (*U*-tests).
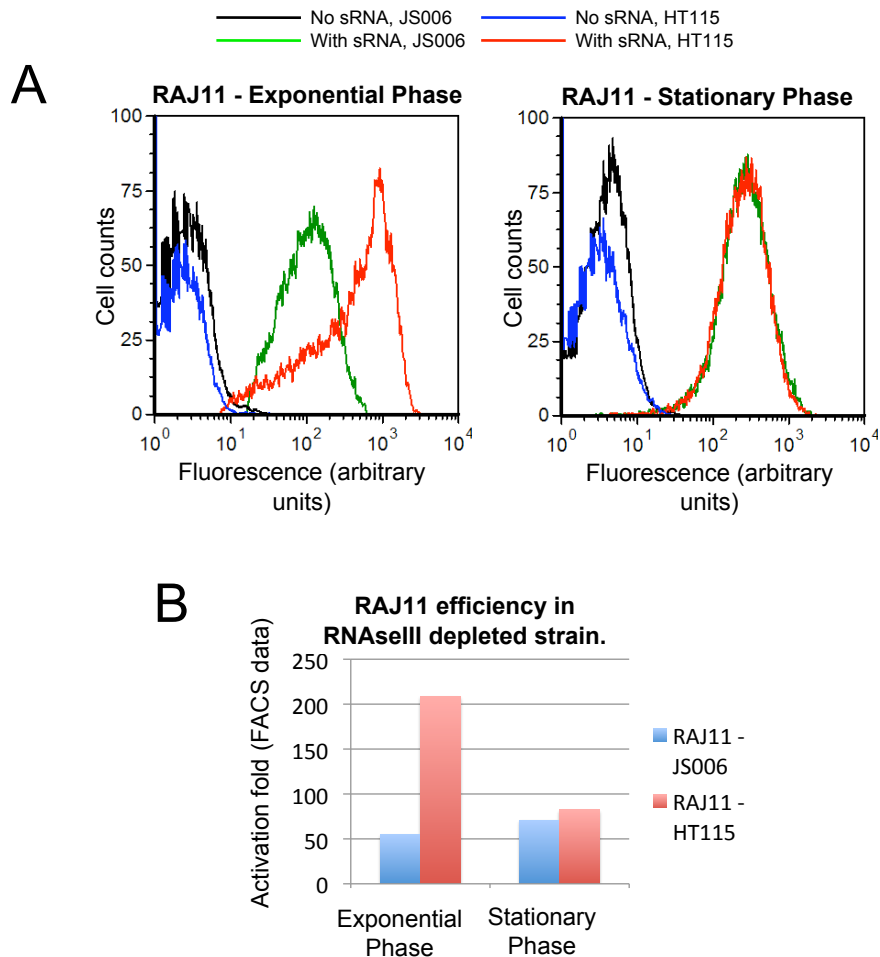
Fig. S16: Flow cytometry analysis to compare the activity of RNA devices in presence and absence of RNase III. (A) Flow-cytometric results of system RAJ11 in strains JS006 and HT115. In exponential phase, the efficiency of system RAJ11 is significantly increased in HT115 strain. (B) The apparent activation fold (according to FACS data) of system RAJ11 in HT115 (209x) presents a 4-fold increase compared to the one in JS006 (55x).
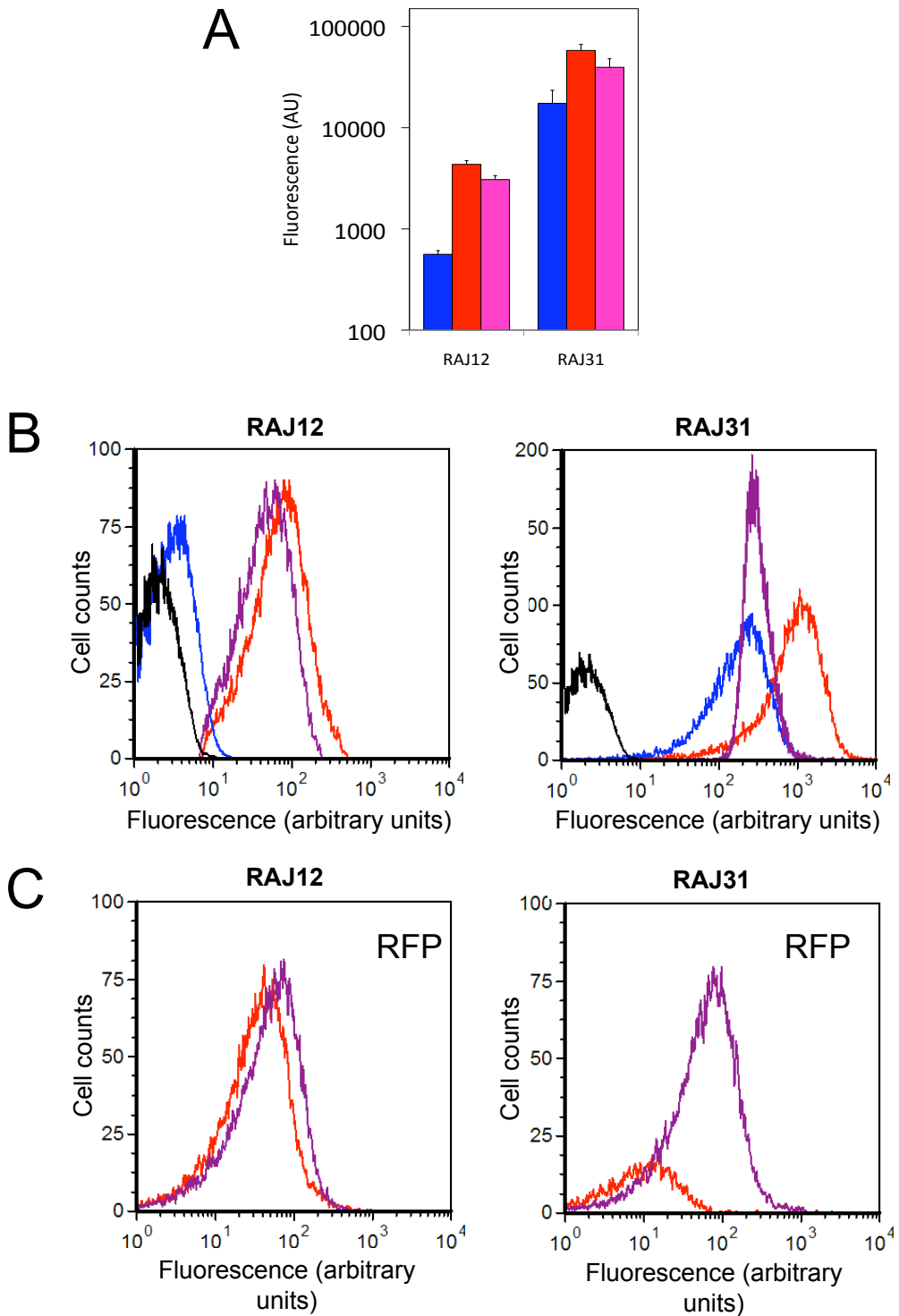
Fig. S17: Effect of the transcription terminator on the performance of the riboregulator, according to (A) fluorometry and (B) flow cytometry. Magenta bars / distributions show the fluorescence activated by riboregulators without terminator (blue and red bars / distributions follow the color map of Fig. 3A / S15). In both cases (devices RAJ12 and RAJ31), we have a significant reduction of fluorescence between the red and magenta bars / distributions (U-test, $P<0.05$). Arguably, because in absence of an efficient terminator the thermodynamic ensemble of riboregulators has a much higher variability and then the set of functional configurations is reduced. (C) RFP fluorescence distributions showing an increase of it when removing the terminator (see Fig. S2).

A

Systems	Geometric Mean (FITC)
Positive Control (Green)	2931.04
Negative Control (Black)	1.40
RAJ11 (Red)	98.67
RAJ11 – no sRNA (Blue)	1.78
RAJ12 (Red)	65.89
RAJ12 – no sRNA (Blue)	1.99
RAJ21 (Red)	13.38
RAJ21 – no sRNA (Blue)	1.29
RAJ22 (Red)	13.54
RAJ22 – no sRNA (Blue)	1.49
RAJ23 (Red)	15.98
RAJ23 – no sRNA (Blue)	4.34
RAJ31 (Red)	591.85
RAJ31 – no sRNA (Blue)	101.63

B

Growth Phase	Systems	Mean
Exponential Phase	RAJ11 JS006 (Green)	98.67
	RAJ11 – no sRNA JS006 (Black)	1.78
	RAJ11 HT115 (Red)	350.70
	RAJ11 – no sRNA HT115 (Blue)	1.68
Stationary Phase	RAJ11 JS006 (Green)	233.44
	RAJ11 – no sRNA JS006 (Black)	3.30
	RAJ11 HT115 (Red)	196.40
	RAJ11 – no sRNA HT115 (Blue)	2.39

C

Systems	Mean (FITC)
Positive Control (Green)	2931.04
Negative Control (Black)	1.40
RAJ12 (Red)	65.89
RAJ12 – no terminator (Purple)	44.11
RAJ12 – no sRNA (Blue)	1.99
RAJ31 (Red)	591.85
RAJ31 – no terminator (Purple)	306.08
RAJ31 – no sRNA (Blue)	101.63

Systems	Mean (Cy5)
RAJ12 (Red)	19.87
RAJ12 – no terminator (Purple)	21.41
RAJ31 (Red)	1.56
RAJ31 – no terminator (Purple)	32.42

Fig. S18: Geometric means corresponding to the flow cytometry distributions shown in Fig. S15 (A), Fig. S16 (B), and Fig. S17 (C).
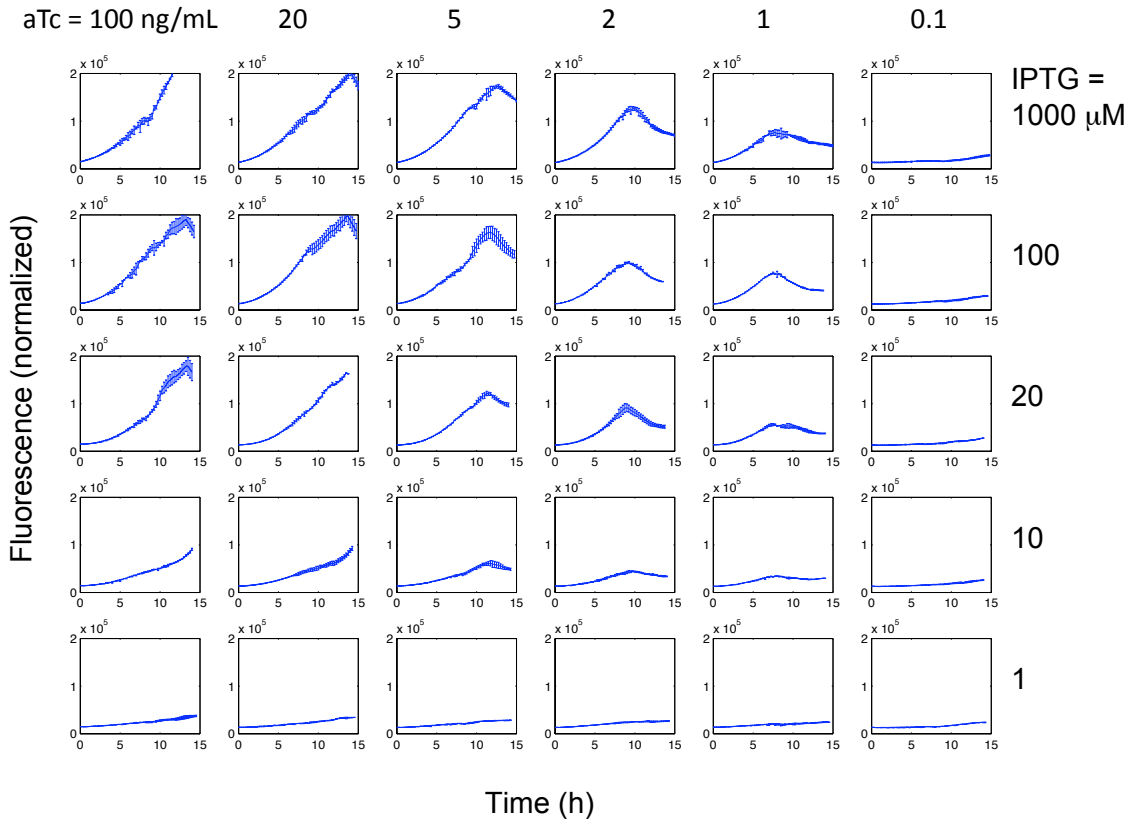
Fig. S19: Dynamical characterization of the AND logic gate circuit based on transcription and post-transcription control. To implement this circuit, we used the system RAJ11. IPTG and aTc were introduced at time 0. Herein, normalized fluorescence is the ratio between fluorescence and OD_{600}.
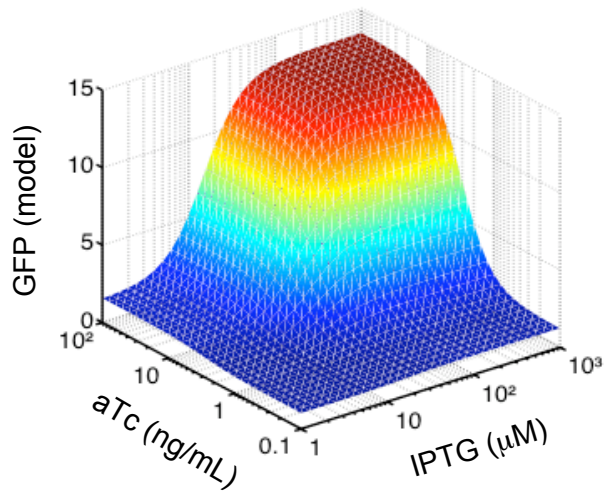
Fig. S20: Computationally predicted transfer function (in steady state) of the circuit (see also Fig. 5C for the prediction of experimental values) using Eq. S7.

ΔG = -14.7 ; α = 8 (trans-trans)
ΔG = -13.6 ; α = 10 (trans-trans-cis)
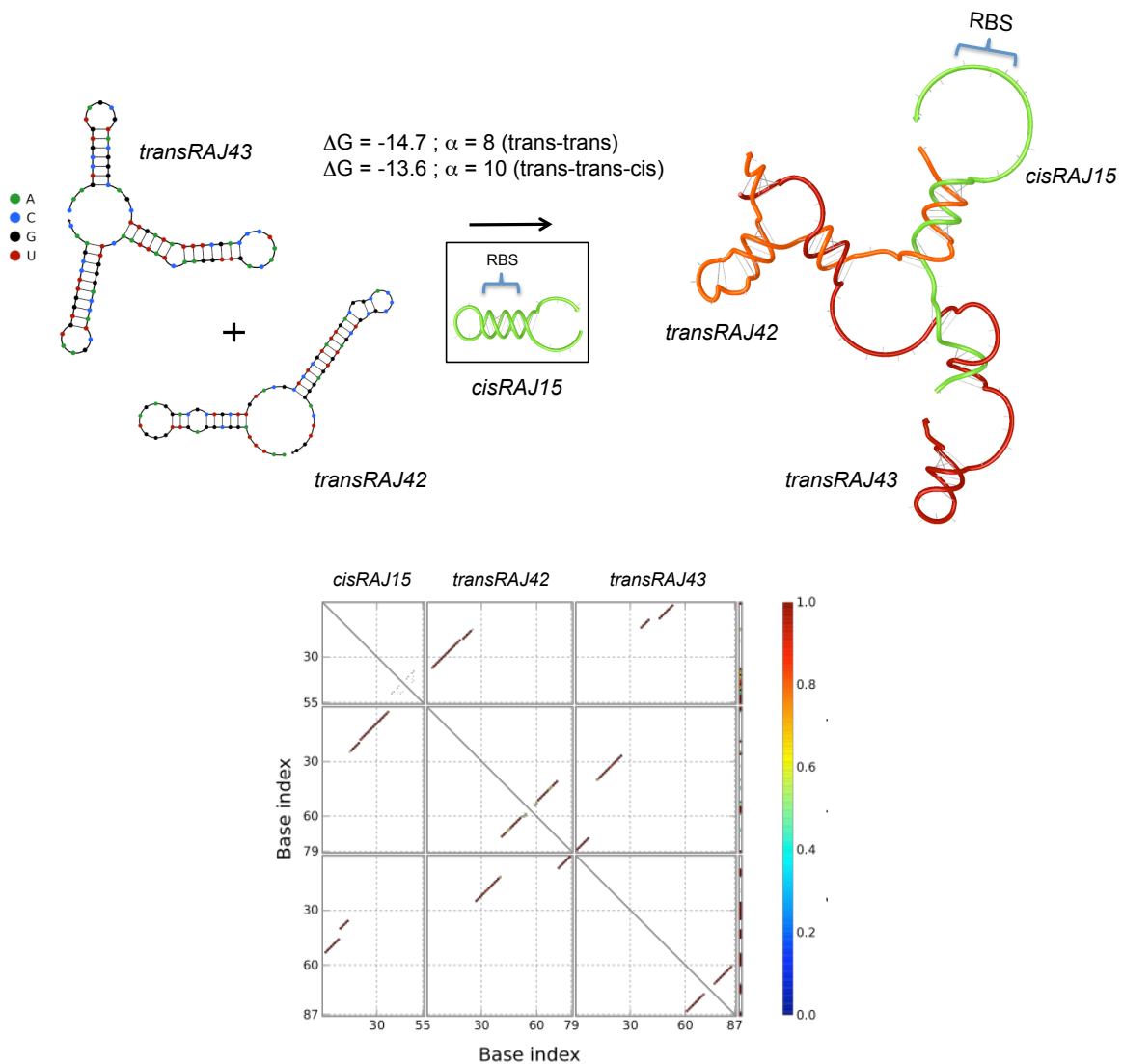
Fig. S21: Computational design of synergistic riboregulators. In the small inset we show the helical structure of the cis-regulating RNA (cisRAJ15). We show the helical structure of the three-RNA-strand complex cisRAJ15::transRAJ42::transRAJ43, showing the release of the RBS, together with the corresponding base-pairing probability matrix. The sequences are shown in Table S10.

Supporting Tables

Table S1: Sequences (of DNA) computationally designed of the *cis*-repressing RNAs (labeled as cisRAJi) and *trans*-activating RNAs (labeled as transRAJi), together with their MEC. For *cis*-repressing RNA, we highlight in blue the ribosome binding site (RBS) and in green the starting codon ATG. For *trans*-activating RNA, we also show the sequences of the transcription terminators (BioBrick identifiers B0015 and B1002) used in this work.

```
>cisRAJ11 (specification: C1 structure)
CCTCGCATAATTTCACTTCTTCAATCCTCCCGTTAAAGAGGAGAAATTATGAATG
......(((((((((.((((((.(((......))).)))))))).)))))))).....
```

```
>transRAJ11 (specification: T4 structure)
GGGAGGGTTGATTGTGTGAGTCTGTCACAGTTCAGCGGAAACGTTGATGCTGTGACAGATTTATGCGAGGC
..........((((((((((((((((((((((((....)))))).)))))))))))))))))))))...
```

```
>cisRAJ12 (specification: C1 structure)
ACCCAGTATCATTCTCTTCTTCCTGCCCACGCGGAAAGAGGAGAAAGGTGTAATG
......((((.(((((((((((.(((.....))).))))))))))).)))).....
```

```
>transRAJ12 (specification: T4 structure)
GGGCAGGAAGAAGGGTTCCTTTGAGCGAATCTAGCGGCACCTCGCTAGGATTTGCTCGAAGGGATTCTGGG
..........((((((((((((((((((((((((....))))))).))))))))))))))))))))...
```

```
>cisRAJ21 (specification: C1 structure)
CCCTGCCTAGTATCTCTTCTTTGCTTCCTCCAGTAAAGAGGAGATATTGGTTATG
......(((((((((((((((((((.....))))))))))))))))))))).....
```

```
>transRAJ21 (specification: T1 structure)
TGGAGGAGAGAGCGATCCTAGTTCTCACTCAAAGAAGGGTAGGACTAGGCAGGGC
...........((..((((((((((.((((.....))))))))))))))).)..))
```

```
>cisRAJ22 (specification: C1 structure)
GCCGTCAACTTGTTTCTTCTTTGGCCCACACGTTAAAGAGGAGATAAGTTTAATG
......(((((((((((((((((((.....))))))))))))))))))))).....
```

```
>transRAJ22 (specification: T2 structure)
GACGTGTTAGCGGGCCAAAGATTGCTAGTTGACGGCTGATGCTTGAGTATGATAGTAGTTTATACTCAGGTGTACTAAG
....((((((((.(((.........))).))))))))....(((((((((((((.......)))))))))))))......
```

```
>cisRAJ23 (specification: C1 structure)
GTGTCGGTTGTATTTCTTCTTTAGGCACCCTCTTAAAGAGGAGATGTAATGTATG
......(((((((((((((((((((.....))))))))))))))))))))).....
```

```
>transRAJ23 (specification: T3 structure)
GGAGGGTCGCCTAAAGCGATTTGTTTGCTCCCGCGTTCATACCTAGGATGTGTGGAGCAGATCGGTCATAAGGGATATGAT
CGATAT
...(((((((.....)))))))...((((((((((((.......)))))))).)))))).((((((((((.....))))))
)))))..
```

```
>cisRAJ31 (specification: C1 structure)
AGTGGATATGCTTTACCTCTTGGTGAGACGACATAAAGAGGAGAAACATAATATG
......((((.(((.((((((.(((.....))).)))))))).)))).)))))....
```

```
>transRAJ31 (specification: T5 structure)
ACATCAAACGTCCAGCGCCTGGGTCGTAGTTATGTGGTAAATGGTTGCTAGGATCAATATTAAGCTTTACCGTCGTCTCAT
CCGCAATTAAGTCCCTATCCGCTGTCACTGTATTGGTCTTAGTAGCTATTTGCTACATGGCTACGATCTTTTTTT
....................(((((((((((((((((((((((((((((((((((((..(((...............
...................)))......)))))))))))))))))))))))))))))))))))))))))......
```

```
>positive control
AACTAGAGAAAGAGGAGAAACTAGATG
```

```
>negative control
ATCAGCAGGACGCACTGACCATG
```

```
>BBa_B0015
ccaggcatcaaataaaacgaaaggctcagtcgaaagactgggcctttcgttttatctgttgtttgtcggtgaacgctctct
actagagtcacactggctcaccttcgggtgggcctttctgcgtttata
```

```
>BBa_B1002
cgcaaaaaaccccgcttcggcggggttttttcgc
```

23

Table S2: Structures of the *cis*-repressing and *trans*-activating RNAs when forming the active complex, showing the release of the RBS (in blue) to allow ribosome docking (pseudoknots are represented by [ ], in case of system RAJ31).

```
>cisRAJ11
CCUCGCAUAAUUUCACUUCUUCAAUCCUCCCGUUAAAGAGGAGAAAUUAUGAAUG +
(((((((((((..((((....(((((((((((....................... +
GGGAGGGUUGAUUGUGUGAGUCUGUCACAGUUCAGCGGAAACGUUGAUGCUGUGACAGAUUUAUGCGAGGC
)))))))))))....)))).(((((((((((((((((....)))))).)))))))))).)))))))))).
>cisRAJ12
ACCCAGUAUCAUUCUCUUCUUCCUGCCCACGCGGAAAGAGGAGAAAGGUGUAAUG +
.((((((.(((...((((((((((((((............................ +
GGGCAGGAAGAAGGGUUCCUUUGAGCGAAUCUAGCGGCACCUCGCUAGGAUUUGCUCGAAGGGAUUCUGGG
))))))))))))))))..(((((((((((((((((((....)))))).)))))))))))))))).)))))
>cisRAJ21
CCCUGCCUAGUAUCUCUUCUUUGCUUCCUCCAGUAAAGAGGAGAUAUUGGUUAUG +
(((((((((((..(((((((((..((((((....................... +
UGGAGGAGAGAGCGAUCCUAGUUCUCACUCAAAGAAGGGUAGGACUAGGCAGGGC
)))))))(((((.......))))))...)))))))))))....))))))))))).
>cisRAJ22
GCCGUCAACUUGUUUCUUCUUUGGCCCACACGUUAAAGAGGAGAUAAGUUUAAUG +
((((((((((.((....(((((((((((((((((..................... +
GACGUGUUAGCGGGCCAAAGAUUGCUAGUUGACGGCUGAUGCUUGAGUAUGAUAGUAGUUUAUACUCAGGUGUACUAAG
.)))))))....))))))))))..)).))))))))))..(((((((((((((((.......)))))))))))))))......
>cisRAJ23
GUGUCGGUUGUAUUUCUUCUUUAGGCACCCUCUUAAAGAGGAGAUGUAAUGUAUG +
(((((((((..(((..((((((((((((((((((..................... +
GGAGGGUCGCCUAAAGCGAUUUGUUUGCUCCCGCGUUCAUACCUAGGAUGUGUGGAGCAGAUCGGUCAUAAGGGAUAUGAUCG
AUAU
.))))))).))))))))).(((..((((((((((((((((.......))))))).)))))))))))))))..)))..)))..)))..)))))
))).
>cisRAJ31
AGUGGAUAUGCUUUACCUCUUGGUGAGACGACAUAAAGAGGAGAAACAUAAUAUG +
[[[[[[[[.[[[[........[[[[[[[[[[[[..................... +
ACAUCAAACGUCCAGCGCCUGGGUCGUAGUUAUGUGGUAAAUGGUUGCUAGGAUCAAUAUUAAGCUUUACCGUCGUCUCAUCC
GCAAUUAAGUCCCUAUCCGCUGUCACUGUAUUGGUCUUAGUAGCUAUUUGCUACAUGGCUACGAUCUUUUUUU
....................((((((((((((((((((((((((((((((((((((...........]]]]]]]]]]].
......]]]]...]]]]]]]]......))))))))))))))))))))))))))))))))))))))......
```

Table S3: Sequences (5' sense) of the toeholds in the designs. To compute this we avoid GU pairs. We also show an alignment with the 5' YUNR motif (in blue) and calculate a simple metric of similarity. ΔG_{up} represents the free energy in the RNA-RNA interaction computed with RNAup from ViennaRNA package (36).

	cisRAJ	transRAJ	YUNR motif	$-\Delta G_{up}$ (Kcal/mol)
11	CCUCCC -YUNY-	GGGAGG	75%	17.4
12	CCC YCN	GGG	50%	9.6
21	UCCUCC --YUNY	GGAGGA	75%	11.9
22	GCC	GGC NR-	50%	7.5
23	CCCU --YU	AGGG	50%	6.6
31	AGACGA	UCGUCU UNR---	75%	16.2

Table S4: Thermodynamic properties of the designed RNA devices. The probability for specificty is estimated from the concentration of the complex in the equilibrium. The probability for RBS releasing is estimated from the ensemble of structures and the partition function.

Device	-ΔG (Kcal/mol)	-G_{cis} (Kcal/mol)	-G_{trans} (Kcal/mol)	Specificity	RBS releasing
RAJ11	17.2	15.0	40.0	99%	95%
RAJ12	15.6	19.2	36.4	97%	92%
RAJ21	15.0	24.6	17.0	95%	88%
RAJ22	17.5	21.2	24.5	98%	97%
RAJ23	20.2	15.4	32.9	100%	98%
RAJ31	14.1	13.4	56.4 0 (only loop)	100%	80%

Table S5: Computational prediction of orthogonality between the designed RNA devices. We show the equilibrium concentrations of the complex in %, assuming equal initial concentrations of the single RNA molecules. We used 1 μM for each species. In case of RAJ31, we considered the loop of the *trans*-RNA to avoid pseudoknots ([*] this value increases to 4.72 when considering the whole sequence). The average specificity of cognate pairs (S_{cog}) is computed as the average value of the elements in the diagonal of the matrix, giving S_{cog}=97.00%. The average specificity of non-cognate pairs ($S_{non-cog}$) is computed as the average value of the elements out of the diagonal of the matrix, giving $S_{non-cog}$=1.88%. The degree of orthogonality (O) of these devices is computed as O=(S_{cog}-$S_{non-cog}$)/S_{cog}=0.9809.

trans *cis*	RAJ11	RAJ12	RAJ21	RAJ22	RAJ23	RAJ31 (loop)
RAJ11	99.20	0.02	2.47	0	1.31	0
RAJ12	2.40	96.63	0.14	0	0.14	0.02 [*]
RAJ21	4.96	42.69	94.80	0	0.32	0
RAJ22	0.09	1.21	0.04	98.48	0.01	0
RAJ23	0	0.05	0	0.01	99.88	0.40
RAJ31	0	0	0	0	0	99.92

Table S6: Computational prediction of similarity of the designed riboregulators with natural small non-coding RNAs. We used BLASTN against the database NONCODE of non-coding RNAs involving 411,552 sequences (39).

Riboregulator	Alignment versus bacterial ncRNAs	Alignment versus all ncRNAs (report of highest similarity)	*De novo* design
transRAJ11	No significant match *E*-val>2	32 bits, AK016545, *Mus musculus*, *E*-val=1.3	YES
transRAJ12	No significant match *E*-val>2	32 bits, AK017976, *Mus musculus*, *E*-val=1.3	YES
transRAJ21	No significant match *E*-val>2	32 bits, AF440362, *Balamuthia mandrillaris*, *E*-val=0.96	YES
transRAJ22	No significant match	32 bits, AK136693, *Mus musculus*, *E*-	YES

	E-val>2	val=1.5	
transRAJ23	No significant match E-val>2	32 bits, AK137975, *Mus musculus*, E-val=1.7	YES
transRAJ31	No significant match E-val>2	36 bits, AK048256, *Mus musculus*, E-val=0.22	YES

Table S7: Estimation of the explored sequence space. L is the number of nucleotides to be mutated in the structure, P the number of base-pairs between nucleotides to be mutated, and H the number of hairpins. Then, Ω is an estimation of the average number of sequences with a common structure according to the formula $\Omega = 0.67$ $L^{1.5}$ 2.16^L (29). C is a structure-related parameter computed as C = (L+P)/H. F is a structural factor fitted with the data shown in (40), being $F = 3(C/L)^{12.9}$. A prediction of the number of sequences with a common structure is $\Omega^* = F\Omega$. S is the simple estimation of the number of sequences according to $S = 4^{L-P}$. To estimate the length of the sequence space of the whole system, we need to account for all sequence spaces corresponding to the species of the system. For instance, in the case of the device RAJ11, the structures C2 and T4 were used, hence we have $\sim10^{40}$ possible sequences to be explored (using the values of Ω^*).

Structure	L	P	H	Ω	C	Ω^*	S
C1	26	7	1	$\sim10^{10}$	33	$\sim10^{12}$	$\sim10^{11}$
T1	55	16	1	$\sim10^{20}$	71	$\sim10^{22}$	$\sim10^{23}$
T2	79	24	2	$\sim10^{29}$	52	$\sim10^{27}$	$\sim10^{33}$
T3	87	23	3	$\sim10^{31}$	37	$\sim10^{27}$	$\sim10^{38}$
T4	71	24	1	$\sim10^{26}$	95	$\sim10^{28}$	$\sim10^{28}$
T5	40	0	0	$\sim10^{15}$	-	-	$\sim10^{24}$

Table S8: Rational redesign of one RNA device (RAJ11) to obtain orthogonal systems (RAJ11b, RAJ11c and RAJ11d), based on key mutations (in blue) over the toehold sequence (in red).

```
>cisRAJ11
CCUCGCAUAAUUUCACUUCUUCAAUCCUCCCGUUAAAGAGGAGAAAUUAUGAAUG

>cisRAJ11b
CCUCGCAUAAUUUCACUUCUUCAAUCGUGCCGUUAAAGAGGAGAAAUUAUGAAUG

>cisRAJ11c
CCUCGCAUAAUUUCACUUCUUCAAUCUUUCCGUUAAAGAGGAGAAAUUAUGAAUG

>cisRAJ11d
CCUCGCAUAAUUUCACUUCUUCAAUGGUCCCGUUAAAGAGGAGAAAUUAUGAAUG
```

```
>transRAJ11
GGGAGGGUUGAUUGUGUGUGAGUCUGUCACAGUUCAGCGGAAACGUUGAUGCUGUGACAGAUUUAUGCGAGGC

>transRAJ11b
GGCACGGUUGAUUGUGUGUGAGUCUGUCACAGUUCAGCGGAAACGUUGAUGCUGUGACAGAUUUAUGCGAGGC

>transRAJ11c
GGAAAGGUUGAUUGUGUGUGAGUCUGUCACAGUUCAGCGGAAACGUUGAUGCUGUGACAGAUUUAUGCGAGGC

>transRAJ11d
GGGACCGUUGAUUGUGUGUGAGUCUGUCACAGUUCAGCGGAAACGUUGAUGCUGUGACAGAUUUAUGCGAGGC
```

Specificity results (as computed in Table S5):

	transRAJ11	transRAJ11b
cisRAJ11	99.9	<0.01

cisRAJ11b	1.55	97.8

	transRAJ11	transRAJ11c
cisRAJ11	99.9	<0.01
cisRAJ11c	47.8	67.3

	transRAJ11	transRAJ11d
cisRAJ11	99.9	0.02
cisRAJ11d	1.55	76.5

Table S9: Values of normalized fluorescence (NF), growth rate (μ) and translation rate (TR), which is calculated with the third equation in Eqs. S6 in steady state, for the designed RNA devices. That is, TR = NF $(\mu+\delta_g)$ $(1+(\mu+\delta_g)/m)$, where m = 0.132 min^{-1} (41) and δ_g = 0.0005 min^{-1} (42). * indicates that growth rate is calculated after an initial transient period where cells grow irregularly.

Strain	Normalized fluorescence (AU)	Growth rate (h^{-1})	Translation rate (AU/min)
JSRAJ11	5,216	0.17	17.8
JSRAJ11m	465	0.27	2.4
JSRAJ12	4,339	0.10*	9.6
JSRAJ12m	561	0.23	2.5
JSRAJ21	1,057	0.19	4.0
JSRAJ21m	384	0.14*	1.1
JSRAJ22	1,940	0.19	7.3
JSRAJ22m	697	0.19	2.6
JSRAJ23	2,680	0.09	5.4
JSRAJ23m	946	0.17	3.2
JSRAJ31	58,014	0.21	239.1
JSRAJ31m	17,401	0.17	59.5
HTRAJ11	46,159	0.14*	133.6
HTRAJ11m	1,730	0.12	4.4

Table S10: Sequences (of DNA) computationally designed of the *cis*-repressing RNA and *trans*-activating RNAs in system presented in Fig. S21.

```
>cisRAJ15 (specification: C1 structure)
TGTTCCGACGGGTCTCCTCTTTCGACTCCGCTTGAAAGAGGAGATTTGTCATATG

>transRAJ42 (specification: T2 structure)
AATTTAGGCGGAGTTGGGTAGAGGACGCTGCTTGTACGCTCTCGTATTGACGGCACCCGCGTCGATGTGAGGGACTTGG

>transRAJ43 (specification: T3 structure)
CAAGTCCGTGTAGCGTACGGGCAGCTTGATATTTCGACCCTAACAGTTGGAACTATTAACTTGGGACCATCGAATGTGGTT
CCGAAC
```

Table S11: Strains and plasmids used in this study. We provide the reference to the plasmids deposited in AddGene (http://www.addgene.org).

Strains or plasmids	Features	Ref.	AddGene Ref.
Escherichia coli TOP10	Commercial (Invitrogen)	-	
E. coli K-12 JS006	MG1655 ΔaraC ΔlacI	43	
E. coli K-12 HT115	W3110 rnc-14::Tn10	44	
E. coli K-12 MG1655-Z1	MG1655 lacIQ, PN25-tetR, SpR	45	
pSTC0	pMB1 Ori	This work	39240
pSTC0r1	pSTC0, no 5'-UTR, gfpmut3b	This work	39242
pSTC0r0	pSTC0, RBS-, gfpmut3b	This work	39243
pSTC1	pSC101 Ori	This work	39241
pRAJ11m	RAJ11, pSTC0, no sRNA, gfpmut3b	This work	39245
pRAJ11	RAJ11, pSTC0, sRNA- BBa_B0015, gfpmut3b	This work	39244
pRAJ12m	RAJ12, pSTC1, no sRNA, sfgfp	This work	39247
pRAJ12	RAJ12, pSTC1, sRNA- BBa_B1002, sfgfp	This work	39246
pRAJ12f	RAJ12, pSTC1, sRNA, no terminator, sfgfp	This work	39248
pRAJ21m	RAJ21, pSTC0, no sRNA, gfpmut3b	This work	39250
pRAJ21	RAJ21, pSTC0, sRNA- BBa_B0015, gfpmut3b	This work	39249
pRAJ22m	RAJ22, pSTC0, no sRNA, gfpmut3b	This work	39252
pRAJ22	RAJ22, pSTC0, sRNA- BBa_B0015, gfpmut3b	This work	39251
pRAJ23m	RAJ23, pSTC0, no sRNA, gfpmut3b	This work	39254
pRAJ23	RAJ23, pSTC0, sRNA- BBa_B0015, gfpmut3b	This work	39253
pRAJ31m	RAJ31, pSTC1, no sRNA, sfgfp	This work	39256
pRAJ31	RAJ31, pSTC1, sRNA- BBa_B1002, sfgfp	This work	39255
pRAJ31f	RAJ31, pSTC1, sRNA, no terminator, sfgfp	This work	39257
pRAJ11-12	transRAJ11, cisRAJ12, pSTC1, sfgfp	This work	39258
JS0r1	*E. coli* K-12 JS006, pSTC0r1	This work	
JS0r0	*E. coli* K-12 JS006, pSTC0r0	This work	
JSRAJ11m	*E. coli* K-12 JS006, pRAJ11m	This work	
JSRAJ11	*E. coli* K-12 JS006, pRAJ11	This work	
JSRAJ12m	*E. coli* K-12 JS006, pRAJ12m	This work	
JSRAJ12	*E. coli* K-12 JS006, pRAJ12	This work	
JSRAJ12f	*E. coli* K-12 JS006, pRAJ12f	This work	
JSRAJ21m	*E. coli* K-12 JS006, pRAJ21m	This work	
JSRAJ21	*E. coli* K-12 JS006, pRAJ21	This work	
JSRAJ22m	*E. coli* K-12 JS006, pRAJ22m	This work	
JSRAJ22	*E. coli* K-12 JS006, pRAJ22	This work	
JSRAJ23m	*E. coli* K-12 JS006, pRAJ23m	This work	
JSRAJ23	*E. coli* K-12 JS006, pRAJ23	This work	
JSRAJ31m	*E. coli* K-12 JS006, pRAJ31m	This work	
JSRAJ31	*E. coli* K-12 JS006, pRAJ31	This work	
JSRAJ31f	*E. coli* K-12 JS006, pRAJ31f	This work	
JSRAJ11-12	*E. coli* K-12 JS006, pRAJ11-12	This work	
HT0r1	*E. coli* K-12 HT115, pSTC0r1	This work	
HT0r0	*E. coli* K-12 HT115, pSTC0r0	This work	
HTRAJ11m	*E. coli* K-12 HT115, pRAJ11m	This work	
HTRAJ11	*E. coli* K-12 HT115, pRAJ11	This work	
MGZRAJ11	*E. coli* K-12 MG1655-Z1, pRAJ11	This work	

Supporting Datasets

Dataset S1 (in xls format) contains the raw data from fluorometry experiments to characterize our RNA devices.

Supporting References

1. Lutz R, Bujard H (1997) Independent and tight regulation of transcriptional units in Escherichia coli via the LacR/O, the TetR/O and AraC/I1-I2 regulatory elements. *Nucl. Acids Res.* **25**, 1203-1210.

2. Strainic MG Jr *et al.* (2000) Promoter interference in a bacteriophage lambda control region: effects of a range of interpromoter distances. *J. Bacteriol.* **182**, 216-220.

3. Cormack BP, *et al.* (1996) FACS-optimized mutants of the green fluorescent protein (GFP). *Gene* **173**, 33-38.

4. Pédelacq J-D, *et al.* (2003) Engineering and characterization of a superfolder green fluorescent protein. *Nat. Biotechnol.* **24**, 79-88.

5. Shetty RP, Endy D, Knight TF Jr (2008) Engineering BioBrick vectors from BioBrick parts. *J. Biol. Eng.* **2**, 5.

6. Sambrook J, Fritsch EF, Maniatis T. *Molecular Cloning: A Laboratory Manual* (Cold Spring Harbor Laboratory Press, New York, 1989).

7. Rozen S, Skaletsky HJ (2000) Primer3 on the WWW for general users and for biologist programmers. *Methods Mol. Biol.* **132**, 365-386.

8. Franke GC, *et al.* (2007) Expression and functional characterization of gfpmut3.1 and its unstable variants in Staphylococcus epidermidis. *J. Microbiol. Methods* **71**, 123-132.

9. Carothers JM, *et al.* (2011) Model-driven engineering of RNA devices to quantitatively program gene expression. *Science* **334**, 1716-1719.

10. Alper H, *et al.* (2005) Tuning genetic control through promoter engineering. *Proc. Natl. Acad. Sci. USA* **102**, 12678-12683.

11. Hao Y, *et al.* (2011) Quantifying the sequence-function relation in gene silencing by bacterial small RNAs. *Proc. Natl. Acad. Sci. USA* **108**, 12473-12478.

12. Carrera J, *et al.* (2011) Empirical model and in vivo characterization of the bacterial response to synthetic gene expression show that ribosome allocation limits growth rate. *Biotechnol. J.* **6**, 773-783.

13. Penchovsky R, Breaker RR (2005) Computational design and experimental validation of oligonucleotide-sensing allosteric ribozymes. *Nat. Biotechnol.* **23**, 1424-1433.

14. Sosnick TR, Pan T (2003) RNA folding: models and perspectives. *Curr. Opin. Struct. Biol.* **13**, 309-316.

15. Brantl S (2002) Antisense-RNA regulation and RNA interference. *Biochim. Biophys. Acta* **1575**, 15-25.

16. Franch T, *et al.* (1999) Antisense RNA regulation in prokaryotes: rapid RNA/RNA interaction facilitated by a general U-turn loop structure. *J. Mol. Biol.* **294**, 1115-1125.

17. Kirkpatrick S, Gelatt CD, Vecchi MP (1983) Optimization by simulated annealing. *Science* **220**, 671-680.

18. Mathews DH, *et al.* (1999) Expanded sequence dependence of thermodynamic parameters improves prediction of RNA secondary structure. *J. Mol. Biol.* **288**, 911-940.

19. Hofacker IL, *et al.* (1994) Fast folding and comparison of RNA secondary structures. *Monatsh. Chem.* **125**, 167-188.

20. Andronescu M, Zhang ZC, Condon A (2005) Secondary structure prediction of interacting RNA molecules. *J. Mol. Biol.* **345**, 987-1001.

21. Dirks RM, *et al.* (2007) Thermodynamic analysis of interacting nucleic acid strands. *SIAM Rev.* **49**, 65-88.

22. Yurke B, Mills AP Jr (2003) Using DNA to power nanostructures. *J. Genet. Prog. Evol. Mach.* **4**, 111-122.

23. Yin P, *et al.* (2008) Programming biomolecular self-assembly pathways. *Nature* **451**, 318-322.

24. McCaskill JM (1990) The equilibrium partition function and base pair binding probabilities for RNA secondary structure. *Biopolymers* **29**, 1109-1119.

25. Das R, Karanicolas J, Baker D (2011) Atomic accuracy in predicting and designing noncanonical RNA structure. *Nat. Methods* **7**, 291-294.

26. Sharma S, Ding F, Dokholyan NV (2008) iFoldRNA: three-dimensional RNA structure prediction and folding. *Bioinformatics* **24**, 1951-1952.

27. Sim AY, Minary P, Levitt M (2012) Modeling nucleic acids. *Curr. Opin. Struct. Biol.* **22**, 273-278.

28. Kingsford C, Ayanbule K, Salzberg SL (2007) Rapid, accurate, computational discovery of Rho-independent transcription terminators illuminates their relationship to DNA uptake. *Genome Biol.* **8**, R22.

29. Schuster P (1995) How to search for RNA structures. Theoretical concepts in evolutionary biotechnology. *J. Biotechnol.* **41**, 239-257.

30. Soloveichik D, Seelig G, Winfree E (2010) DNA as a universal substrate for chemical kinetics. *Proc. Natl. Acad. Sci. USA* **107**, 5393-5398.

31. Bintu L, *et al.* (2005) Transcriptional regulation by the numbers: models. *Curr. Opin. Genet. Dev.* **15**, 116-124.

32. Landrain TE, *et al.* (2009) Modular model-based design for heterologous bioproduction in bacteria. *Curr. Opin. Biotechnol.* **20**, 272-279.

33. Levine E, *et al.* (2007) Quantitative characteristics of gene regulation by small RNA. *PLoS Biol.* **5**, e229.

34. Nakashima N, Tamura N (2009) Conditional gene silencing of multiple genes with antisense RNAs and generation of a mutator strain of Escherichia coli. *Nucl. Acids Res.* **37**, e103.

35. Busch A, Richter AS, Backofen R (2008) IntaRNA: efficient prediction of bacterial sRNA targets incorporating target site accessibility and seed regions. *Bioinformatics* **24**, 2849-2856.

36. Muckstein U, *et al.* (2006) Thermodynamics of RNA-RNA binding. *Bioinformatics* **22**, 1177-1182.

37. Isaacs FJ, *et al.* (2004) Engineered riboregulators enable post-transcriptional control of gene expression. *Nat. Biotechnol.* **22**, 841-847.

38. Qi L, *et al.* (2012) Engineering naturally occurring trans-acting non-coding RNAs to sense molecular signals. *Nucl. Acids Res.* **40**, 5775-5786.

39. Altschul SF, *et al.* (1997) Gapped BLAST and PSI-BLAST: a new generation of protein database search programs. *Nucl. Acids Res.* **25**, 3389-3402.

40. Cowperthwaite MC, *et al.* (2008) The ascent of the abundant: how mutational networks constrain evolution. *PLoS Comput. Biol.* **4**, e1000110.

41. Iizuka R, Yamagishi-Shirasaki M, Funatsu T (2011) Kinetic study of de novo chromophore maturation of fluorescent proteins. *Anal. Biochem.* **414**, 173-178.

42. Andersen JB, *et al.* (1998) New unstable variants of green fluorescent protein for studies of transient gene expression in bacteria. *Appl. Environ. Microbiol.* **64**, 2240-2246.

43. Stricker J, *et al.* (2008) A fast, robust and tunable synthetic gene oscillator. *Nature* **456**, 516-519.

44. Takiff HE, Chen SM, Court DL (1989) Genetic analysis of the rnc operon of Escherichia coli. *J. Bacteriol.* **171**, 2581-2590.

45. Dunlop MJ, *et al.* (2008) Regulatory activity revealed by dynamic correlations in gene expression noise. *Nat. Genet.* **40**, 1493-1498.